14

Application of wavelet transform to describe acoustic emission in the process of material fracture

© V.L. Hilarov, E.E. Damaskinskaya

Ioffe Institute,
St. Petersburg, Russia

E-mail: Vladimir.Hilarov@mail.ioffe.ru

Received September 26, 2025
Revised November 28, 2025
Accepted December 8, 2025

Wavelet analysis of time dependencies of acoustic emission signal amplitudes for heterogeneous materials under mechanical load, as well as earthquake magnitudes in Italy in 1990–2000, is performed. It is shown that the occurrence of large events and destruction of materials is preceded by an increase in energy release at various scale levels. It is concluded that this increase can serve as a predictor of material destruction.

Keywords: materials fracture prediction, wavelet analysis, heterogeneous materials.

DOI: 10.61011/PSS.2025.12.63090.266-25

1. Introduction

The problem of preventing the destruction of man-made structures and forecasting natural and man-made disasters remains very relevant at the present time. A structural health monitoring (SHM) [1] is often used to solve these problems, which allows the identification and localization of damage appearing in materials. One of the methods widely used for this type of monitoring is the acoustic emission (AE) method [2,3 and references therein]. The wavelet transform is widely applied to the analysis of acoustic emission signals, mainly when their waveforms are known (see reviews [4,5]). However, obtaining information about the waveforms of AE signals is extremely difficult for a number of reasons. Firstly, the shape of the waveform is significantly influenced by the design of the piezoelectric transducer, as well as the sensor attachment system to the sample. Secondly, the sensor reacts differently to the incoming wave depending on the angle of its incidence. Therefore, the source type (a crack of a certain size) may be the same, and the waveform that will be recorded by the equipment may be different. Thirdly, the same sensor produces different waveforms from the same sources, but located in different parts of the sample due to spatial dispersion and different attenuation of the frequency components of the AE signal (the path of the wave through the sample will have a significant impact in terms of material heterogeneity). In addition, the waveform is also affected by distortion of the signal due to its reflection from external and internal surfaces (defects, grain boundaries), etc. Therefore, AE data is most often a set of amplitudes and times of acoustic signals, and sometimes contains the coordinates of their sources. This paper is devoted specifically to the study of time series of amplitudes of AE signals.

The main difficulties in analyzing acoustic emission time series are related to the fact that this process is not stationary during the destruction of materials, therefore standard statistical methods such as calculating distribution moments, correlation functions, and spectral analysis are not applicable for them [6]. Indeed, the average values (mathematical expectation, variance, covariance) for non-stationary series are not constant. This leads to the fact that the theorems on consistency and asymptotic normality of sample estimates and their variances are not valid. The distribution functions are different for different samples of the same length. As the sample size increases, the accuracy of estimates does not increase. Therefore, in this paper, the wavelet analysis is used to study nonstationary AE series. Unlike the Fourier transform, where functions of the form $\exp(ix) = \cos x + i \sin x$ are used as basic transformation functions, which are a composition of sine waves with different frequencies and delocalized in space, substantially localized soliton-like functions are used for the wavelet transform. As such a function, we chose a widely used function of the form „sombrero“, constructed from the second derivative of the Gauss function:

$$\psi(x) = \frac{\partial^2}{\partial x^2} \exp\left(-\frac{x^2}{2}\right). \quad (1)$$

The use of localized basis functions leads to the fact that the method of wavelet transformations retains good resolution on different time scales, which is why it is often called a mathematical microscope [7].

It is known that the so-called variance of the wavelet coefficients, determined by the formula (2), can have predictive properties for catastrophic events [8–10].

$$\sigma(i) = \left[\frac{1}{N-1}\sum_{k=1}^{N}\left(w(i,k) - \langle w(i,k)\rangle\right)^2\right]^{1/2}. \quad (2)$$

Here i is the scale factor of the wavelet transform w, k is the spatial coefficient (sets the position of the wavelet in time). The second term in (2) is the average time value of

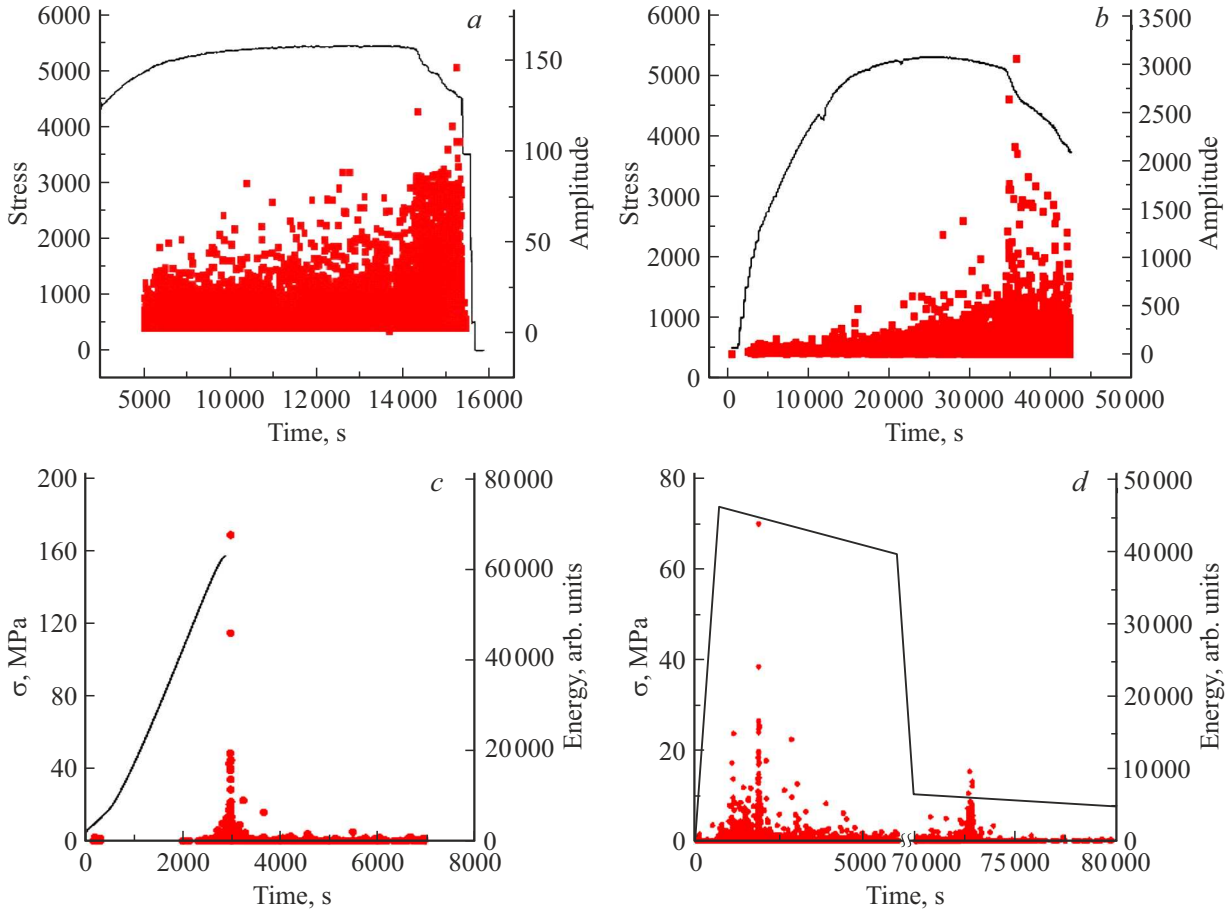

Figure 1. Loading curves (black lines) and energy of acoustic emission signals (red dots) for the experiments under consideration: *a* — sample AE42; *b* — AE43, *c* — Westerly U_Y; *d* — Berea obr4_5800N; *e* — Berea obr2 6000; *f* — Westerly 1P 18 kN; *g* — seismic signal in Italy in 1990–2000.

the wavelet transform, and, as it is easy to show, is zero, due to the fact that the analyzing wavelet has, by definition, a zero average value. By virtue of this, the expression (2) is simply a discrete analogue of the root of the global energy spectrum (3), which will be used later in this work.

$$E(a) = \int w(a,b)^2 db. \qquad (3)$$

Energy (3) depends on the scale a at which the process is studied. Along with (3), the average scale value of this value was also used. It should be noted that we are not talking about spatial scales, but rather about the frequency range. At the same time, high-energy events usually take on large spatial scales and are accompanied by lower-frequency waves. A continuous wavelet transform from the pywt library for Python was used [11].

2. Experimental data

The data obtained in the following experiments were processed in this study: AE42 and AE43 [12], Westerly U_Y. Berea obr4_5800N Berea obr2 6000, Westerly obr 1P [13–15], as well as data on seismic activity in Italy in 1990–2000 in a rectangle with coordinates 36.663-46.89 N; 5.625-18.589 E from the NEIC catalog of the U. S. Geological Survey.

The time dependences of the amplitudes (energies) and the external axial load are shown in Figure 1.

In experiments marked AE42 and AE43 on a deformation control unit (described in more detail in [12]), cylindrical samples ($h = 190.5$ mm, $d = 76.2$ mm) of Westerly granite (AE42) and Harcourt granite (AE43). The samples were deformed under conditions of constant all-round compression (pressure 50 ± 0.2 MPa) and uniaxial axial loading. A system of six piezoelectric transducers (resonant frequency 0.6 MHz) was attached to the sample to register the AE signals generated during loading. As a result of the experiment, a databi ase was obtained in which each AE signal was characterized by the emission time, three hypocenter coordinates, and an amplitude of A reduced to a reference sphere with a radius of $R_f = 10$ mm. The reduced amplitude is the energy characteristic of the signal. The peculiarity of these experiments was that the axial load was changed in such a way that the activity of AE signals

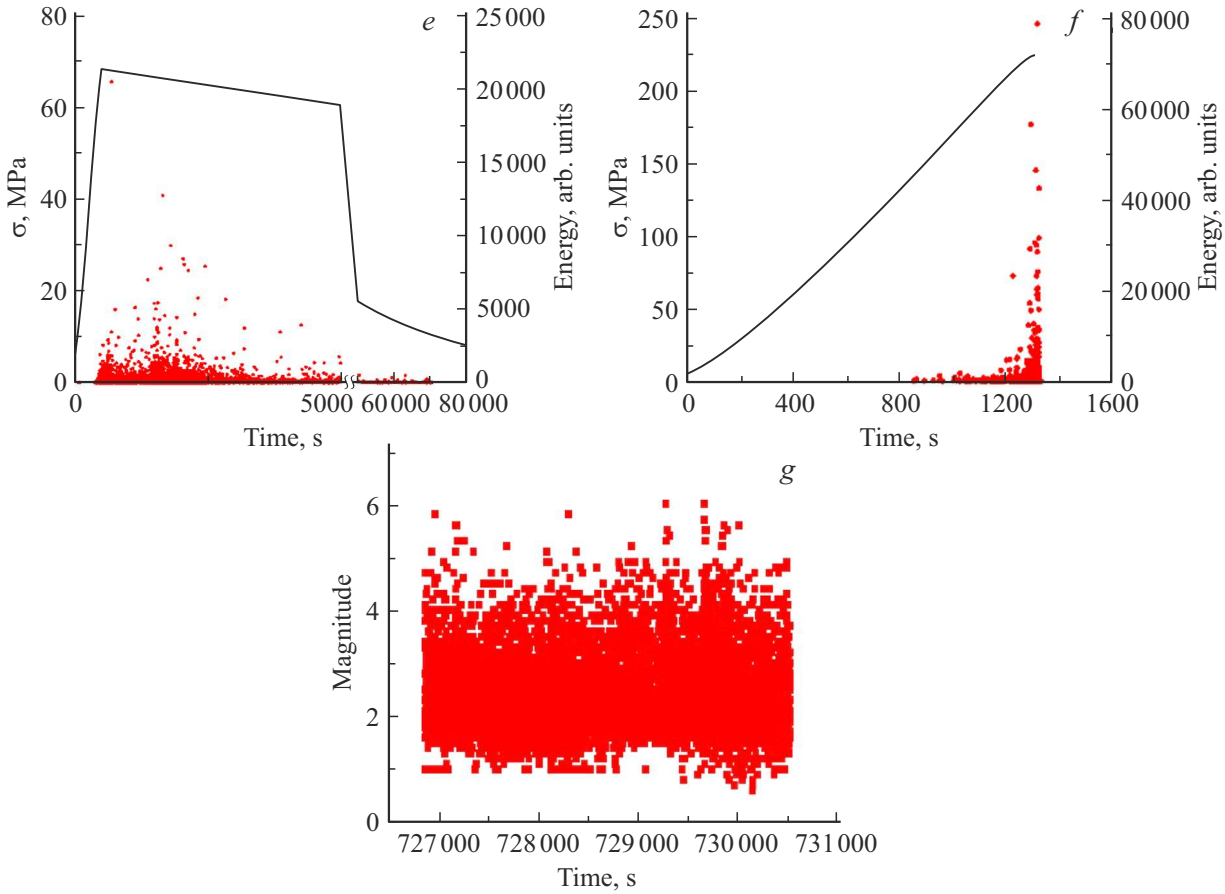

Figure 1 (*continued*).

Sample numbering

Name experiment	AE42	AE43	Westerly U_Y	Berea obr4_5800N	Berea obr2 6000	Westerly 1P 18 kN	Italy
Experiment No.	1	2	3	4	5	6	7
Number of signals	43983	36823	7815	30546	18056	3023	6835

with an amplitude above the threshold did not exceed a predetermined level.

Quasi-static tests of Westerly granite samples (experiments labeled Westerly U_Y and Westerly 1P 18 kN) were carried out under uniaxial compression conditions with a constant velocity of movement of punches 10 μm/min. The Amsy-5 Vallen System hardware system was used to monitor acoustic emissions. Two broadband AE105A acoustic emission piezoelectric transducers with a band of 450–1150 kHz were attached to the ends of the sample. During the experiment, a database was formed in which the parameters of individual AE signals were recorded — the radiation time, the source coordinate, and the energy. With an avalanche-like increase in acoustic emission activity (more than one hundred AE pulses per second), the deformation process was stopped. The criterion used to stop the deformation process, combined with a low deformation rate, allowed, on the one hand, to form a main crack, and, on the other, to preserve the integrity of the sample. AE registration continued after unloading in the Westerly U_Y experiment; AE registration was terminated shortly after loading was stopped in the Westerly 1P 18 kN experiment. These experiments are described in more detail in Refs. [13,14].

The loading program for Berea sandstone samples (experiments labeled Berea obr4_5800N and Berea obr2 6000) consisted of two stages. At the first stage, the sample was subjected to quasi-static uniaxial compression at a loading rate (displacement of the loading plates) of 5 μm/min. Compression was performed up to a force equal to 0.9 of F_{max} (F_{max} is the breaking load determined in preliminary experiments). Then the sample was maintained

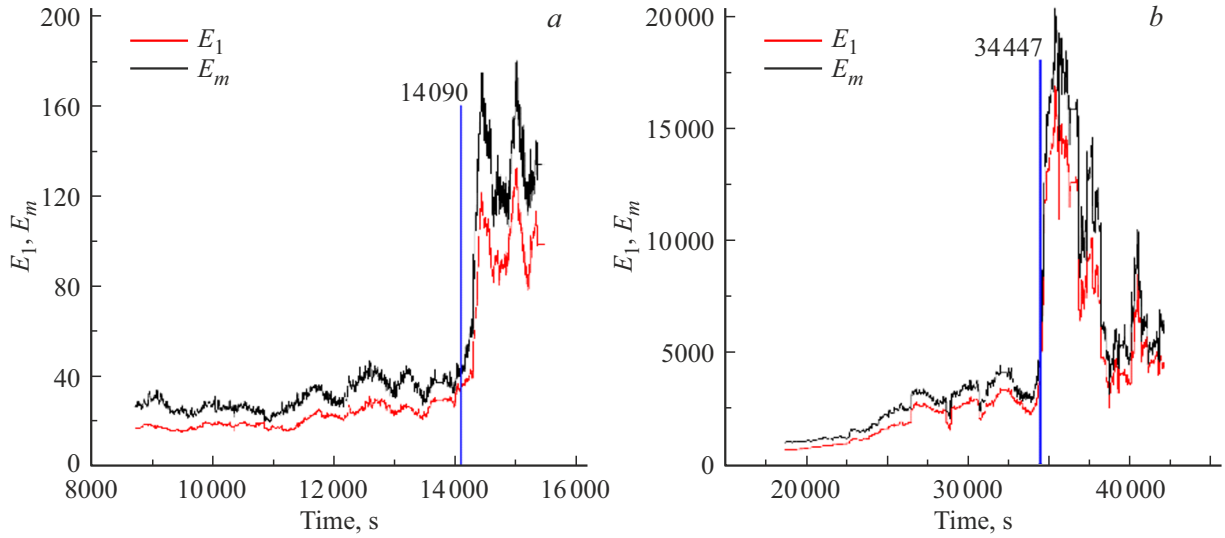

Figure 2. Time dependences of the average global energy of the wavelet transform E_m and the energy of the lower level $E(1) \equiv E_1$: a–f — experiments 1–6; g — dependence of the energy of the lowest scale level for earthquakes in Italy; h — average energy E_m and average energy of events in a sliding window of 512 units E_a. Vertical lines and numbers mark characteristic time points (see text).

under constant deformation until AE decreased to zero. At the same time, the stress on the sample decreased exponentially with time. Acoustic emission was recorded during loading using the Amsy-5 Vallen system (Germany). Two AE105A piezoelectric converters (operating frequency range 450–1150 kHz) were fastened in special hollow cylindrical slabs, used for direct loading of the sample. The experimental setup is described in detail in Ref. [15]. In the future, we will designate these experiments by numbers according to the table. The table also includes the database sizes for each sample.

A defective structure (microcrack system) in the volume was studied in experiments 3–6 by X-ray microtomography using a SkyScan 1172 tomograph (Bruker, Belgium). It was found that a main crack had formed in all the samples, while the samples retained their integrity [13,15].

3. Main results

The acoustic emission and seismic signal data banks were divided into sliding windows of 512–2048 events, depending on the number of signals in the database. A continuous wavelet spectrum and its energy characteristics were calculated in each window. The countdown was attributed to the last event in the window. It should be noted that with this approach, the independent variable is the event number, and the timeline is a function (generally speaking, non-linear) of this number. It should also be noted that as the scale increases, the noise value $E(a)$, calculated using the discrete analog of the formula (3) expression (4), and the scale-averaged energy $E_m = \text{mean}(E(a))$ increased. Therefore, along with the average values of E_m, the value of $E(1)$ was used at the lowest scale level.

$$E(1) \equiv E_1 = \frac{1}{N}\sum_{j=1}^{N} w(1, j)^2. \tag{4}$$

The time dependences of the average energy E_m and energy $E(1)$ for the studied experiments are shown in Figure 2. A common property of all the experiments considered is an increase in the energy characteristics under consideration before the destruction of the sample or a major energy event. Vertical lines with numbers in Figure 2, *a, b* indicate the time point at which the value of the correlation fractal dimension, calculated earlier in Ref. [16], significantly decreases. This decrease, as can be seen from Figure 2, occurs before the value E_m has time to grow significantly. Vertical lines with numbers in Figure 2, c–f mark the times of maximum energy events that occurred during the time period under consideration. It can be seen that each of them is preceded by a significant increase in the values of E_m and $E(1)$. The maximum values of $E(1)$ coincide in time with the times of major earthquakes in the region in Figure 2, *g*. At the same time, the simple windowed average energy value E_a and the scale average E_m in Figure 2, *h* does not have this property. It can also be noted that the main maximum in Figure 2, c–f is preceded by clearly out-of-trend preliminary peaks the times of which are also shown in the figure. Their appearance may be due to the fact that the tendency to macro-destruction appears before the formation of the main maximum, but the process does not develop further, since the energy inflow necessary to continue this process is insufficient. In this case, the model described below can be used to describe the energy balance.

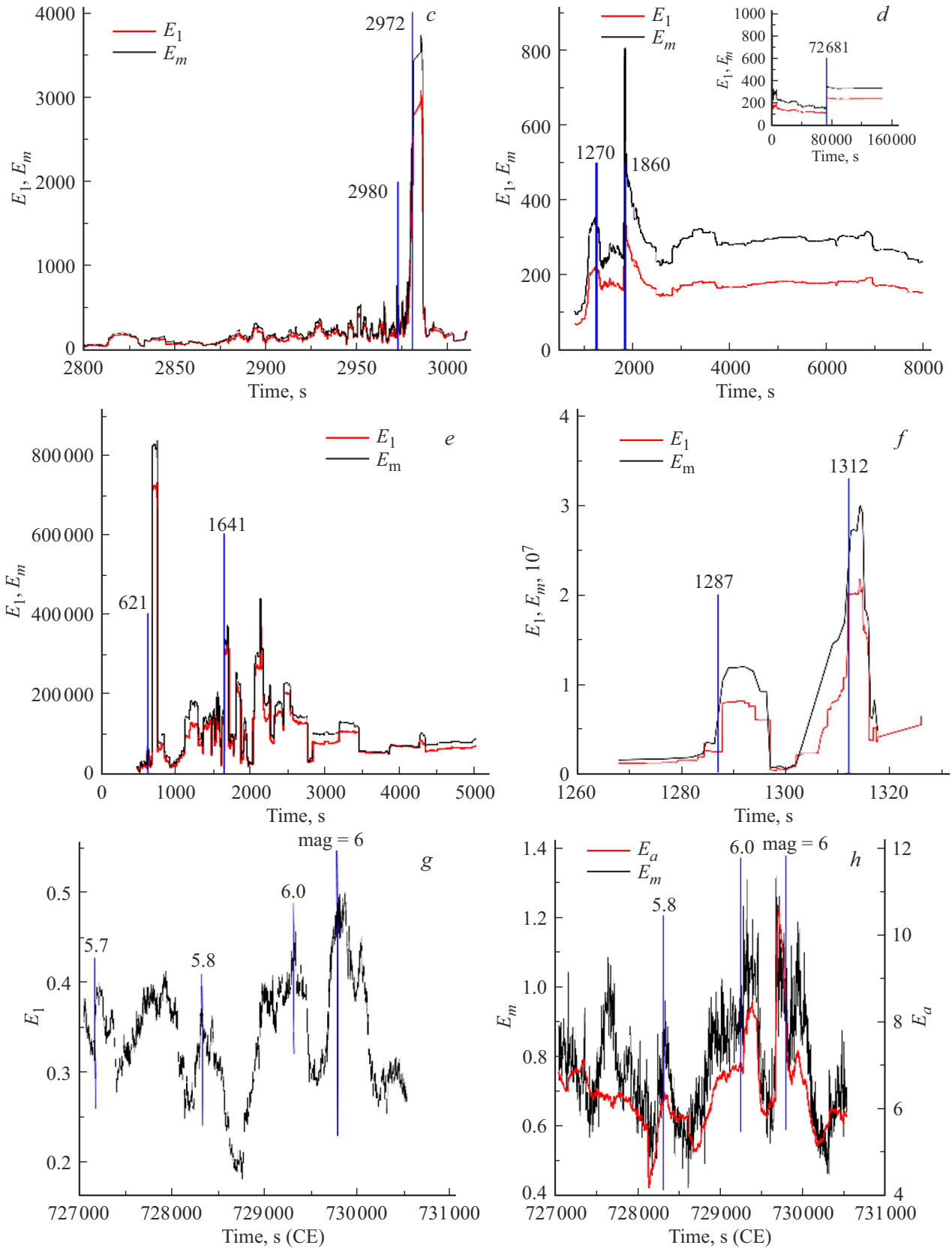

Figure 2 (*continued*).

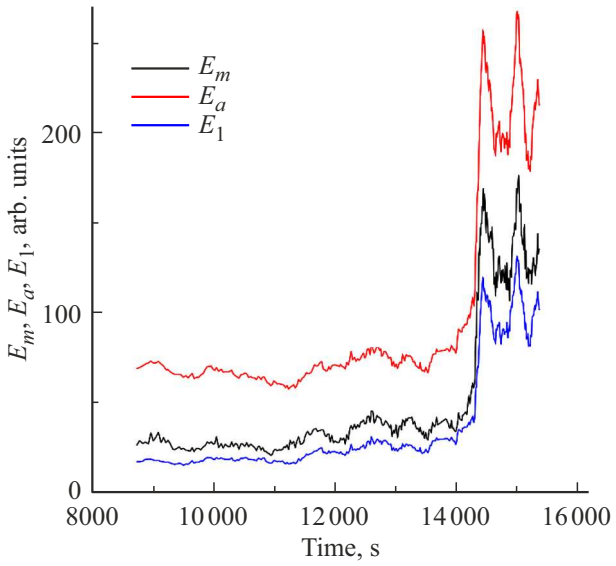

Figure 3. Time dependences of simple windowed energy averages, the averaged global energy spectrum, and the energy of the first scale level for the AE42 experiment.

4. Discussion of the results

An increase in the average energy E_m, as well as its components $E(a)$ before a high-energy event indicates the preparation of large-scale destruction at various scale levels (it should be recalled that here we are not talking directly about spatial scales, but about the frequency range). Thus, significant increases in these values can serve as a predictive sign of an upcoming high-energy event. It would seem that a simple windowed average could also serve as a fracture precursor (Figure 3), but as follows from the comparison of the curves in Figure 2, *g* and Figure 2, *h*, it has this property to a lesser extent. Thus, the times of the maxima of the magnitude $E(1)$ coincide with the times of major earthquakes, while the times of the maxima E_a do not. It follows from this that the time-frequency localization of the wavelet transform has improved predictive properties of high-energy events, and events on lower time scales (high-frequency) play an essential role in predicting destruction.

5. An energy balance model for describing acoustic emission in a heterogeneous material

The considered non-autonomous nonlinear model of the AE energy change over time has the following form:

$$\frac{dE}{dt} = \alpha E\left(1 - \frac{E}{E_{\max}}\right) - \beta E\langle E\rangle_{[t-\tau_1,t-\tau_1/2]} + \gamma\langle E\rangle_{[t-\tau_2,t-\tau_2/2]}\left(1 - \frac{\langle E\rangle_{[t-\tau_2,t-\tau_2/2]}}{E_{\max}}\right) + v_0 \cdot t. \quad (5)$$

The first term of this equation reflects the logistical accumulation of AE energy release (rapid initial growth and further deceleration due to the exhaustion of weak places — initial stress concentrators). This exhaustion of weak places also leads to relaxation of internal stresses with a characteristic time τ_1 and a decrease in the probability of new ruptures, which is described by the second term of the equation. The averaging over the past interval means that the system's memory for previous fracture events. The events that occurred „recently", around the time t, led to stress relaxation and the impossibility, as a result, of new acoustic events in this area. Therefore, the strongest suppression of current activity comes from events that occurred in the middle of the „lull" τ_1. Since the material is usually under the influence of external stresses, energy continues to flow into it, a new redistribution of internal stresses occurs, and new concentrators arise (usually on a larger scale — macro cracks). Therefore, the AE energy release increases again, which is described by the third term of the equation. The relaxation time $\tau_2 > \tau_1$, as it is assumed that the destruction has moved to higher scale levels. The parenthesis in the penultimate term means the restriction that new foci are activated only if the system has not yet reached critical damage. The last term $v_0 \cdot t$ provides an influx of energy from the loading device under the assumption of a linearly time-dependent external force.

The numerical solution of equation (5) is shown in Figure 4 for the zero initial condition $E_0 = 0$ and the following parameter values: $\alpha = 0.15$, $\beta = 0.08$, $\gamma = 0.4$, $\tau_1 = 15$, $\tau_2 = 40$, $E_{\max} = 10$, $v_0 = 0.01$.

It can be seen that the solution in Figure 4 really describes the preliminary maximum observed in the experiments in Figure 2, *c*–*f*. However, it should be noted that depending on the values of the parameters included in (5), these maxima may be several or not at all. Therefore, despite the fact that the model seems reasonable, it is purely descriptive and cannot be used to identify the predictive properties of the destruction of the material. The DEEPSEEK neural

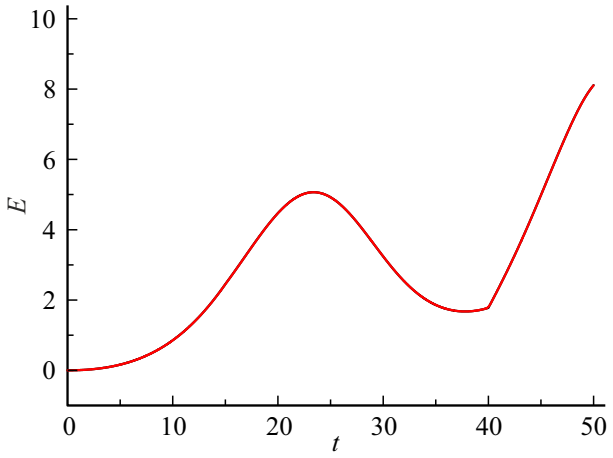

Figure 4. Dependence on the time of AE energy release, obtained as a solution of equation (5).

network participated in the creation of the model. It should be noted that the introduction of asymmetric delay intervals makes it possible to switch from simple AE registration to modeling the internal dynamics of damage in the material, which is a more powerful tool for diagnosis and forecasting. Such models can also be used to describe foreshocks and aftershocks in the Earth's crust.

6. Conclusion

Thus, it has been revealed that before the destruction of materials or large acoustic (seismic) events, energy accumulates on various time scales occure, which can serve as a predictive sign of these events. The use of this predictive feature has an advantage over fractal features such as the Gutenberg-Richter law parameter (b-value), the correlation fractal dimension (d-value), and the change in the width of the multifractal spectrum, since its calculation does not require the use of regression to calculate the parameters and the associated difficulties of automatically selecting the range of scales at which this regression is being performed. At the same time, the d-value change occurs earlier in time. (Figure 2, *a, b*). It is noted that even events on low time scales (high frequency) play an essential role in the prediction of destruction.

It is also noted that in some cases, the main energy maximum is preceded by preliminary maxima that are clearly out of trend, and a kinetic model of energy release describing them is constructed.

Funding

The study was performed under state assignment of Ioffe Institute.

Conflict of interest

The authors declare that they have no conflict of interest.

References

[1] M.A-B. Abdo. Structural Health Monitoring, History, Applications and Future. Open Science Publishers, NY, USA (2014). 115 p.
[2] N.A. Semashko, V.I. Shport, B.N. Maryin. Akusticheskaya emissiya v eksperimental'nom materialovedenii. Mashinostroenie, M. (2002). p. 239 (in Russian).
[3] Md.T. Khan. In: Structural Health Monitoring from Sensing to Processing / Eds. M.A. Wahab, Y.L. Zhou, N.M.M. Maia. Intechopen, L. UK (2018). P. 24–37.
[4] H. Kim, H. Melhem. Eng. Struct. **26**, 347 (2004).
[5] V.R. Skal's'kyi, O.M. Stankevych, I.S. Kuz'. Mater. Sci. **54**, *2*, 139 (2018).
[6] H.E. Stanley, L.A.N. Amaral, A.L. Goldberger, S. Havlin, P.Ch. Ivanov, C.-K. Peng. Physica A **270**, 309–324 (1999).
[7] N.M. Astafieva. UFN **166**, *11*, 1145 (1996) (in Russian).
[8] V.P. Dyakonov. Vejvlety. Ot teorii k praktike. Solon-R, M. (2002). p. 448 (in Russian).
[9] S. Thurner, M.S. Feurstein, M.S. Teich. Phys. Rev. Lett. **80**, 1544 (1998).
[10] I.M. Dremin, V.I. Furletov, O.V. Ivanov, V.A. Nechitailo, V.G. Terziev. A method for diagnosing engine operation, patent No.2154813 (08/20/2000).
[11] G.R. Lee, Ralf Gommers, F. Wasilewski, K. Wohlfahrt, A. O'Leary. J. Open Source Softw. **4**, *36*, 1237 (2019). https://doi.org/10.21105/joss.01237
[12] D.A. Lockner, J.D. Byerlee, V. Kuksenko, A. Ponomarev, A. Sidorin. Nature **350**, 39 (1991).
[13] E.E. Damaskinskaya, V.L. Hilarov, I.A. Panteleyev, D.R. Gafurova, D.I. Frolov. FTT **60**, *9*, 1775 (2018) (in Russian).
[14] E.E. Damaskinskaya, I.A. Panteleev, D.R. Gafurova, D.I. Frolov. FTT **60**, 1353 (2018) (in Russian).
[15] E.E. Damaskinskaya, I.A. Panteleyev, D.V. Korost, K.A. Damaskinsky. FTT **63**, *1*, 103 (2021) (in Russian).
[16] V.L. Hilarov. Modeling Simul. Mater. Sci. Eng. **6**, 337 (1998).

Translated by A.Akhtyamov